Bio-based polymer nanocomposites based on nylon 11 and WS_2 inorganic nanotubes

Mohammed Naffakh,*[a] Peter S. Shuttleworth*[b] and Gary Ellis[b]

Tungsten disulphide nanotubes (INT-WS_2) have been successfully dispersed in a bio-based polyamide matrix (nylon 11) by conventional melt processing. The effect of INT-WS_2 content on the morphology, thermal stability, crystallization behaviour and dynamic mechanical properties is investigated. The results indicate that these inorganic nanotubes can be efficiently incorporated into the bio-based polymer matrix without the need for modifiers or surfactants. Additionally, it is found that the non-isothermal crystallization behaviour of nylon 11/INT-WS_2 depends on both the cooling rate and INT-WS_2 concentration. In particular, crystallization kinetics results demonstrate that the nucleating activity of INTs plays a dominant role in accelerating the crystallization of nylon 11. This fact leads to the appearance of the more-disordered phase at higher temperature. More significantly, it was shown that these INT-WS_2 nanocomposites can facilitate a good processability and cost efficiency, and will be of interest for many eco-friendly and medical applications.

1. Introduction

The discovery of tungsten disulphide (WS_2) fullerene-like particles and nanotubes in thermally sulfurized tungsten films has opened a new field of inorganic solid state chemistry.[1,2] In the following years, a number of new nanotubes and fullerene-like nanoparticles have been synthesized from a variety of compounds with layered (2D) nanostructures, including transition metal disulfides (*e.g.*, MoS_2, NbS_2, TaS_2, TiS_2, and ReS_2), transition metal oxides (*e.g.*, Cs_2O, Tl_2O) and halides (*e.g.*, CdI_2), BN nanotubes, and many others. Various synthetic strategies have been developed or adapted for the synthesis of these nanostructures, including laser ablation, self-assembly, template synthesis, hydrothermal reactions, metal–organic chemical vapour deposition (MOCVD), spray pyrolysis, microwave induced plasmas, gas–solid reactions and fluidized bed reactors. Detailed accounts of such developments can be found in a series of recent review articles.[3–6] Careful investigation of the growth mechanisms of IF-WS_2 and INT-WS_2 resulted in the synthesis of a pure phase and paved the way for larger-scale production, and subsequent understanding of their intrinsic properties and applications.[7,8] In particular, their surprisingly high impact resistance and superior tribological behaviour open up a wide variety of opportunities for applications in catalysis, rechargeable batteries, drug delivery, solar cells and electronics,[5,6] and, more recently, in the field of polymer nanocomposites.[9,10] In addition, INT-WS_2 (or IF-MoS_2) are low-cost, environmentally friendly and biocompatible nanofillers with much lower cytotoxicity than other nanoparticles, such as silica or carbon black.[11]

Taking advantage of their properties, inorganic nanotubes (INT-WS_2) have been recently used as reinforcing agents to improve the thermal, mechanical and tribological properties of isotactic polypropylene,[12] epoxy,[13] electrospun poly(methyl methacrylate) fibers[14] and poly(propylene fumarate) (PPF), the latter for bone tissue engineering.[15] INT-WS_2 have also been successfully dispersed in conducting polymer matrices for application as LED materials[16] as well as to improve the crystallization of poly(3-hydroxybutyrate) (PHB) and poly(L-lactic acid) (PLLA) biopolymer nanocomposites as highly efficient nucleating agents.[17,18] Promising results were also obtained with respect to the thermal, mechanical and tribological behaviour of high-performance biomaterials like poly(ether ether ketone) (PEEK, OPTIMA).[19]

In recent years, polyamide (PA) 11, or nylon 11, has become one of the most promising environmental engineering plastics within the automotive and fuel industries *etc.* due to the fact that it is 100% derived from renewable castor oil[20] and is biocompatible, but not biodegradable under normal conditions.[21] In addition, this promising bio-based polymer possesses excellent piezoelectric behaviour and good cryogenic, oil and water resistance properties, albeit with relatively poor impact, tensile strength and thermal properties.[22] Nano-reinforcement of nylon 11 with carbon nanotubes, nanoclay, cellulose nanofibers, graphene oxide, *etc.* has been shown to be a promising route to overcome these limitations.[23–27] For example, Huang *et al.* reported a 54% increase in the storage modulus compared to that of neat nylon 11 by incorporating 2 wt% multiwalled carbon nanotubes.[23] For nylon 11 filled with

[a]*Escuela Técnica Superior de Ingenieros Industriales, Universidad Politécnica de Madrid (ETSII-UPM), José Gutiérrez Abascal 2, 28006 Madrid, Spain. E-mail: mohammed.naffakh@upm.es*

[b]*Instituto de Ciencia y Tecnología de Polímeros (ICTP-CSIC), Juan de la Cierva 3, 28006 Madrid, Spain. E-mail: peter@ictp.csic.es*

5 wt% organically modified clay an increase of 40% in the tensile modulus and 30% in modulus was observed *via* nano-indentation.[24] Nanocomposites from nylon 11 and 8 wt% dried cellulose nanofibers showed a 41% increase in Young's modulus,[25] and a graphene oxide/nylon 11 nanocomposite prepared by *in situ* melt polycondensation resulted in a 38% increase in the Young's modulus.[26]

It is important to note that the presence of nanofillers have an important influence on the morphology, crystalline structure, and degree of crystallinity of semicrystalline bioplastics, and the final physical and mechanical properties of the matrix will be inevitably affected upon the addition of nanofillers. Tetrapod-shaped zinc oxide whiskers (T-ZnOw) were found to be an ideal reinforcement material due to its special shape and its single crystalline character,[27] and the morphologies of the impact-fractured surfaces of the nanocomposites showed the development of a "terrace" structure and stress whitening when an external force was applied. Finally, in order to control the rate of crystallization and degree of crystallinity, and to obtain the desired morphology and properties of nylon 11, considerable effort has been devoted to characterising its material properties and crystallization kinetics.[28]

The purpose of this study is to address the structure–property–performance relationship of a new family of nanocomposites that comprise nylon 11 and WS_2 inorganic nanotubes in order to explore new opportunities in the preparation and development of advanced nanomaterials using conventional, industrially viable processing methods: the most simple, cost-effective and ecologically friendly being the melt-processing route. In particular, the processability and dispersion of INT-WS_2 will be considered when evaluating thermal, structural and mechanical properties of these new nanocomposites.

2. Experimental section

2.1. Materials and processing

The biopolymer matrix, nylon 11 was purchased from Sigma Aldrich Co. (density = 1.026 g cm^{-3}, M_w = 201.31 g mol^{-1}). Multiwall WS_2 1D nanotubes (INT-WS_2) with diameters of 30–150nm and lengths of 1–20 μm were obtained from Nano-Materials Ltd (Israel). Transmission electron microscopy (TEM) analysis of one such nanotube has showed that the typical INTs are 50–100 nm thick made of 20–30 layers with the interlayer spacing of about 0.62 nm.[13,14] Each mixture of nylon 11 and INT-WS_2 (0.1, 0.5 and 1.0 wt%) was dispersed in a small volume of ethanol and homogenized by mechanical stirring and bath ultrasonication for approximately 10 min. Subsequently, the dispersion was partially dried in vacuum at 60 °C under a pressure of about 70 mbar for 24 h. Melt-mixing of the resulting dispersions was performed using a micro-extruder (Thermo-Haake Minilab system) operated with a rotor speed of 100 rpm at 205 °C for 10 min.

2.2. Characterization techniques

2.2.1. Scanning electron microscopy (SEM). The dispersion of INT-WS_2 in the nylon 11 matrix was characterized using an ultra-high field-emission scanning microscopy (FESEM) (SU8000, Hitachi Co., Japan). Cryogenically fractured surfaces from film specimens were coated with a ~5 nm Cr layer to avoid charging during electron irradiation.

2.2.2. Thermogravimetric analysis (TGA). The thermal stability of the nylon 11/INT-WS_2 nanocomposites was analyzed in a TA Instruments Q50 thermobalance using a heating rate of 10°C min^{-1} from 100 to 800 °C in inert (nitrogen) atmosphere with a flow rate of 60 ml min^{-1}.

2.2.3. Differential scanning calorimetry (DSC). The crystallization behaviour of the nanocomposites was investigated using a Perkin Elmer DSC7/Pyris differential scanning calorimeter (Perkin-Elmer España SL, Madrid, Spain), calibrated with indium (T_m = 156.6 °C, ΔH_m = 28.45 kJ kg^{-1}) and zinc(T_m = 419.47 °C, ΔH_m = 108.37 kJ kg^{-1}). Samples of approximately 10 mg were studied in aluminium capsules under an inert nitrogen atmosphere with a flow rate of 25 ml min^{-1}.

In the non-isothermal crystallization process, the sample was first held at 205 °C for 5 min to eliminate any previous thermal history, and then cooled at rates of 2, 5, 10, 15 and 20 °C min^{-1}. The exothermal curves of heat flow as a function of temperature were recorded to analyse the non-isothermal crystallization process of the neat nylon 11 and its nanocomposites.

2.2.4. Wide-angle X-ray diffraction (WAXD). Wide-angle X-ray diffraction measurements (WAXD) were undertaken with a Bruker D8 Advance diffractometer (Bruker AXS GmbH, Karlsruhe, Germany) using Ni-filtered Cu Kα radiation. Difractograms were collected at a scan speed of 0.2° s^{-1} with a resolution of 40 points per degree over the angular region 2θ between 5 and 35°. A thermally controlled chamber was employed to study the dynamic crystallization and melting behaviour of the nanocomposites. Each sample was first held at 205 °C for 5 minutes to erase any thermal history and then cooled from 205 °C to 40 °C at a scanning rate of approx. 4 °C min^{-1}. The samples were then heated from 40 °C to 205 °C at the same scanning rate.

2.2.5. Dynamic mechanical analysis (DMA). Dynamic mechanical analysis of the samples was performed using a Mettler DMA861 in tensile mode on rectangular shaped bars of dimensions 20 × 4 × 0.5 mm^3 in the temperature range between −100 and 150 °C at a heating rate of 3 °C min^{-1} and frequencies of 0.1, 1 and 10 Hz. A dynamic force of 8 N oscillating at fixed frequency and an amplitude of 17 μm were used.

3. Results and discussion

3.1. Morphology and dispersion of INT-WS_2 in the nylon 11 matrix

It is well-known that the dispersion of nanoparticles within a polymer matrix can have a significant influence on the final properties of the material. Fig. 1 shows the morphologies of as-received INT-WS_2 (Fig. 1a and b) and the nylon 11/INT-WS_2 nanocomposites incorporating different concentrations of INT-WS_2 up to 1.0 wt%. As can be seen, the diameters of the INT-WS_2 range from 30–160 nm and they are 1–20 μm in length. Fig. 1c–h illustrates the SEM morphology of the cryo-fractured surfaces of nylon 11/INT-WS_2 nanocomposites obtained by melt-processing. This strategy yields a good dispersion of INT-WS_2 that are almost

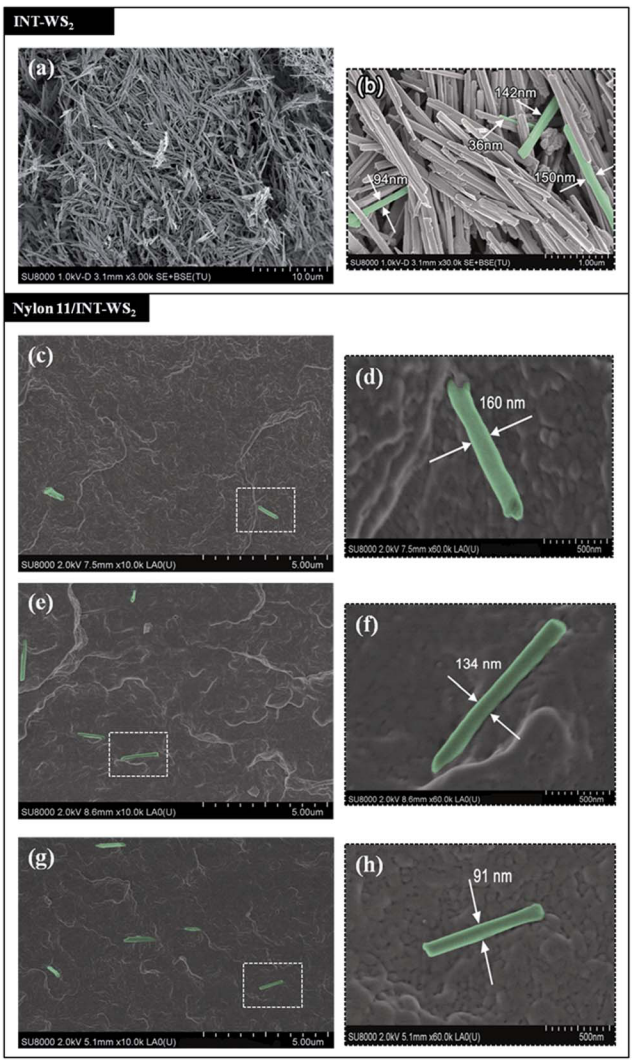

Fig. 1 Low and high magnification high-resolution SEM images of (a and b) WS_2 inorganic nanotubes and nylon 11/INT-WS_2 nanocomposites with (c and d) 0.1, (e and f) 0.5 and (g and h) 1.0 wt% of INT-WS_2. The images highlight the nanotube dimensions (thicknesses) and presence within the samples.

completely debundled into individual tubes within the biopolymer matrix. No aggregation of the INT-WS_2 was detected even at the higher loading of 1.0 wt%. It is important to point out that the INT-WS_2 did not require any special exfoliation or modification methods, making it possible to obtain new bionanocomposite formulations without the complexity and processing costs associated with such treatments.

Wide-angle X-ray diffraction (WAXD) measurements were performed on film samples obtained directly from a hot-press to determine whether the addition of INT-WS_2 affects the crystalline structure of nylon 11. Fig. 2 shows the diffractograms obtained from neat nylon 11 and its nanocomposites with different INT-WS_2 concentrations. At room temperature only the characteristic diffraction peaks of nylon 11 (ref. 29) and INT-WS_2 (ref. 7) are seen. For nylon 11, the three main reflections at $2\theta = 7.2$, 20.2, 23.08 correspond to (001), (100) and (010/110) planes, respectively, of the triclinic α-form.[29] The results indicate that the addition of INTs does not modify the crystal structure of nylon 11, and that nylon in all the nanocomposites crystallizes in the stable α-form.

3.2. Thermal stability of nylon 11/INT-WS_2

The thermal stability of neat nylon 11 and its nanocomposites was investigated by TGA under a nitrogen atmosphere. Although INTs present a high inherent thermal stability,[14] analysis of the thermograms revealed that the INT-WS_2 had no influence on the characteristic degradation temperatures of nylon 11. Thus, the temperature at 10% weight loss (T_{10}) and that corresponding to the maximum rate of weight loss (T_{mr}) appeared at the same temperatures as the neat nylon 11 matrix, approximately 397 °C and 437 °C, respectively.

3.3. Non-isothermal crystallization and temperature evolution of crystal structure

Fig. 3 shows the DSC cooling curves of nylon 11 and the nylon 11/INT-WS_2 nanocomposites obtained at various cooling rates ranging from 2 to 20 °C min^{-1}, corresponding to temperature changes that are found habitually in industrial applications. From these curves, the crystallization peak temperature (T_p) and enthalpy (ΔH_c) were obtained to describe the non-isothermal crystallization behaviour. In all of the thermograms a single exothermic peak was observed upon cooling. The crystallization peak for both the neat nylon 11 and the nanocomposites broadens as the cooling rate increases and the T_p shifts to a lower temperature, indicating that the lower the cooling rate the earlier crystallization occurs. When the samples are cooled quickly from the melt, the motion of the polymer chains does not follow the cooling rate and more supercooling is required to initiate crystallization.

However, the most striking result was the influence of the concentration of INT-WS_2 on the crystallization exotherms of nylon 11 at a particular cooling rate. The crystallization peak temperatures (T_p) of nylon 11/INT-WS_2 nanocomposites were observed to be higher than those of pure nylon 11, indicating an increase in the crystallization rate of nylon 11 due to the

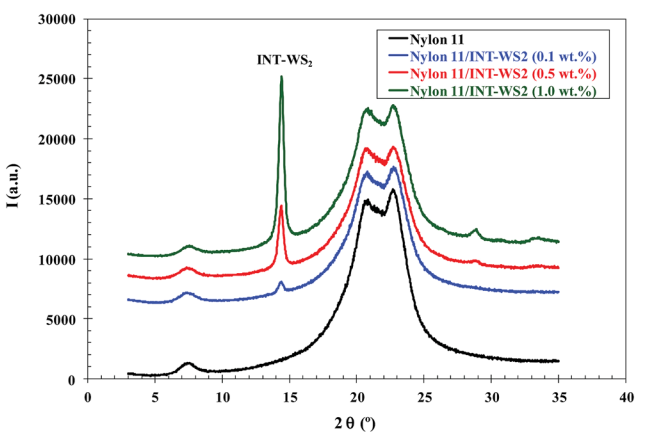

Fig. 2 WAXD diffractograms of melt-processable of nylon 11/INT-WS_2 nanocomposites obtained at room temperature.

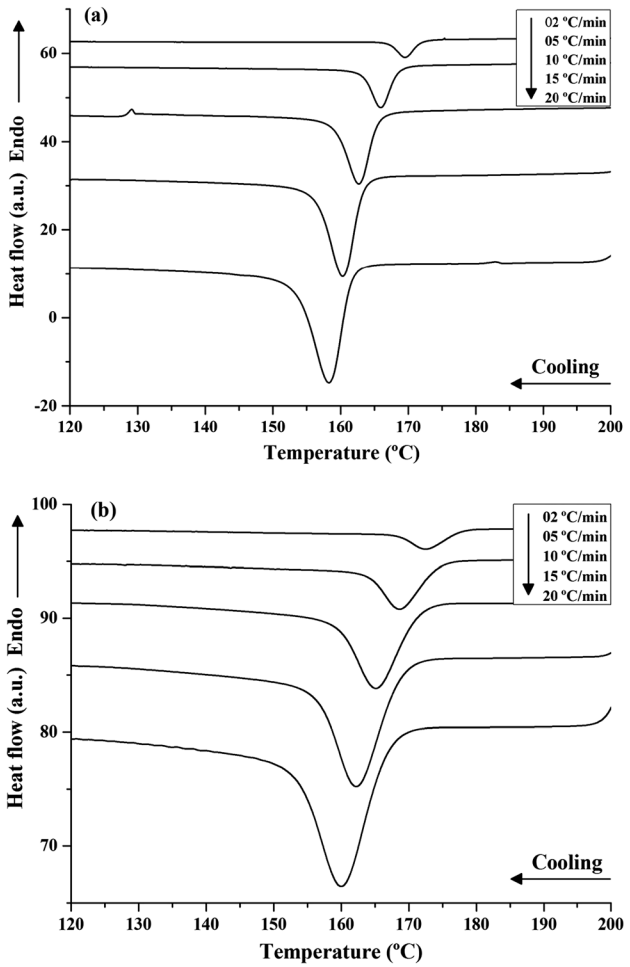

Fig. 3 DSC thermograms of the dynamic crystallization of (a) pure nylon 11, (b) nylon 11/INT-WS_2 (1.0 wt%) at the cooling rates indicated.

presence of INT-WS_2. For more clarity, Fig. 4 shows the variation of T_p with cooling rate and composition. With increasing cooling rate, T_p decreased, indicating that crystallization at higher cooling rates was faster (Fig. 4a). Additionally, the T_p value of nylon 11/INT-WS_2 nanocomposites was slightly higher than that of neat nylon 11 at a given cooling rate. This effect was clearly observed to be a function of the composition, Fig. 4b, manifesting in an increase of around 4 °C with 1.0 wt% of INT-WS_2 at a cooling rate of 2°C min^{-1}. This suggests that INT-WS_2 acts as a heterogeneous nucleating agent increasing the crystallization rate. Likewise, the crystallization enthalpy ΔH_c of nylon 11/INT-WS_2 was not only affected by the cooling rate, with increased cooling rates promoting ΔH_c (Fig. 5a), but also by the INT-WS_2 loading. This variation in the ΔH_c for nylon 11 with different INT-WS_2 concentrations can be clearly seen in Fig. 5b, where the addition of INT-WS_2 induces a decrease in the ΔH_c. Addition of 0.1 wt% INT-WS_2 to nylon 11 produced a decrease in ΔH_c of up to 11% compared to that of pure nylon 11. This effect was observed to be a function of composition, with for example, at 10°C min^{-1} the ΔH_c decreasing by 10% and 16% at INT-WS_2 concentrations of 0.1 wt% and 0.5 wt% respectively, levelling-off at 18% for the highest concentration of 1.0 wt%.

Different filler types produce different effects on the crystallization behaviour in polymer nanocomposites. Gunes *et al.* studying the crystallization of shape memory polymers illustrated that the effect of nanofillers on crystallization could not be considered as originating from their physical presence alone, but is also influenced by their chemical nature, which can provoke a decrease in crystallinity.[30,31] Wu *et al.* reported that ZnO nanorods physically hindered the motion of nylon 11 chains, retarding crystallization and resulting in a slight T_p decrease.[32] In contrast, other fillers such as cellulose nanofibers,[25] nanoclays (MMT)[33] and multiwalled carbon nanotubes (MWNTs)[34] have been reported to promote the crystallization of nylon 11. In particular, the remarkable increase of the crystallization rate of nylon 11/MMT has shown to have a 'supernucleating' effect, resulting from the nanodispersed clay layers.

It is well-known that polyamides exhibit a complex crystallisation behaviour with temperature and Nylon 11 is not an exception, with the most significant factor controlling the crystalline form being that all possible hydrogen bonds are completely satisfied in linear aliphatic polyamides.[35] To meet this condition, the chains adopt a fully extended configuration (α-form) or a slightly twisted configuration (γ-form) and orient in a parallel or antiparallel fashion, depending upon the number of CH_2 groups in the repeat unit. In the fully extended α-form configuration, hydrogen bonds occur between amides in the same plane as the CH_2 zig-zags, forming one large molecular sheet. This configuration is also associated with the β-form. The only difference in the α- and β-forms is that the α-form molecular sheets are alternatively staggered up and down, whereas in the β-form, the sheets are shifted in one direction.[35] In the twisted configuration or γ-form, amide groups twist 60° out of the plane of the molecular sheet. Zhang *et al.* have studied the crystal form transitions of nylon 11 at different drawing temperatures with different drawing ratios.[29] Similarly, Nair *et al.* provided new information on the polymorphism of nylon 11 using high-temperature WAXS/FTIR.[36] These studies demonstrated that nylon 11 is one of the few nylons that exhibit an extensive degree of polymorphism (*i.e.* α, α′, pseudo-hexagonal phases γ/δ/δ′). In addition, Mollova *et al.* investigated the effect of supercooling/nucleation rate on the generation of different polymorphs using fast scanning chip calorimetry and differential scanning calorimetry.[37] In particular, it was found that crystallization at low supercooling was related to the formation of triclinic α-crystals of lamellar morphology and ringed/banded spherulites. However, at high supercooling, formation of pseudo-hexagonal δ′-mesophase was observed.

Real-time WAXD was employed to monitor the dynamic crystallization process. As an example, Fig. 6a shows the diffractograms of nylon 11 and its nanocomposite with 1.0 wt% INT-WS_2 recorded during cooling from the melt to room temperature. The data appears to suggest that nylon 11 first crystallizes into a pseudo-hexagonal (δ′) phase (reflection at $2\theta \approx 21°$) from the molten state, and then changes into a stable triclinic α-form (characteristic reflections at $2\theta \approx 20°$ and $2\theta \approx 23°$) on further cooling. These results also indicated that the controlled cooling of nylon 11 improved the order of the

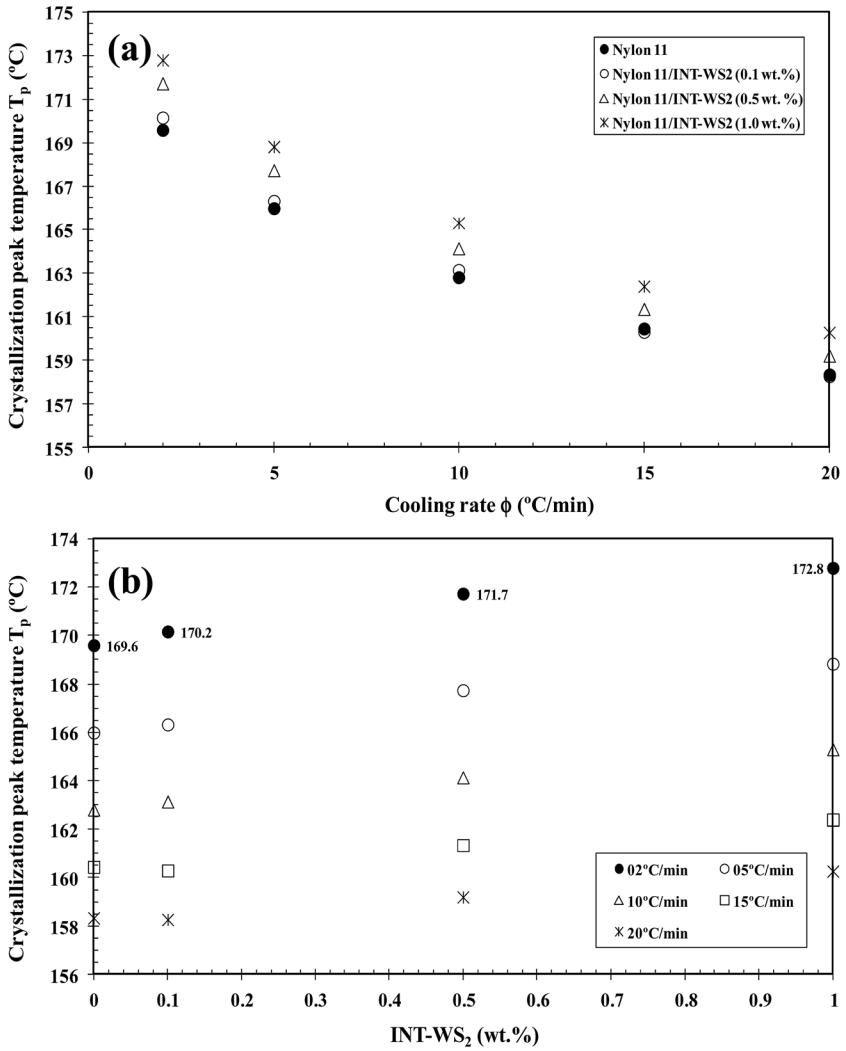

Fig. 4 Variation of the crystallization peak temperature (T_p) for nylon 11/INT-WS_2 nanocomposites with (a) cooling rate and (b) composition.

hydrogen bonds within the sheets and increased the crystal perfection of the polymer. However, in the case of the nanocomposites, which crystallize slightly faster than the pure nylon 11, once the initial energy barrier to nucleation was overcome, the increased fraction of parallel chain–chain conformations may enhance growth of the pseudo-hexagonal phase. This led to the appearance at higher temperature of the more-disordered phase. A more detailed investigation on the effect INTs on the crystalline structure and morphology of nylon 11 is currently underway.

3.4. Nucleation activity

As the crystal form is dependent on the rate of crystallisation it is important to quantify the nucleation activity of INT-WS_2 in the nanocomposites. A common measure of the efficiency of a nucleator is the nucleation activity (φ) that varies from 0 to 1, corresponding to extremely active to inert, respectively. According to Dobreva and Gutzow,[38,39] the nucleation activity can be calculated from the ratio:

$$\varphi = \frac{B^*}{B} \tag{1}$$

where B is a parameter derived from the pristine polymer, and B^* from the polymer/nucleator system. B and B^* can both be experimentally determined from the slope of the following equation:

$$\ln\phi = A - \frac{B(\text{or } B^*)}{\Delta T_p^{\,2}} \tag{2}$$

where ϕ is the cooling rate, A is a constant, ΔT_p is the supercooling ($T_m - T_p$), T_m is the melting point temperature and T_p the crystallization peak temperature. In Fig. 7, eqn (2) is represented for neat nylon 11 and its nanocomposites, considering a value of 202.8 °C for the thermodynamic equilibrium melting temperature of nylon 11.[40] The values of B and B^* are obtained from the slope of the fitted lines, and the nucleation activity (φ) is calculated from this ratio. The values of φ were determined to be 0.90, 0.78 and 0.71 for an INT-WS_2 concentration of 0.1, 0.5 and 1.0 wt%, respectively. The smaller values of φ indicate a nucleating effect of INT-WS_2 on the crystallization of nylon 11. Moreover, the nucleation activity of the

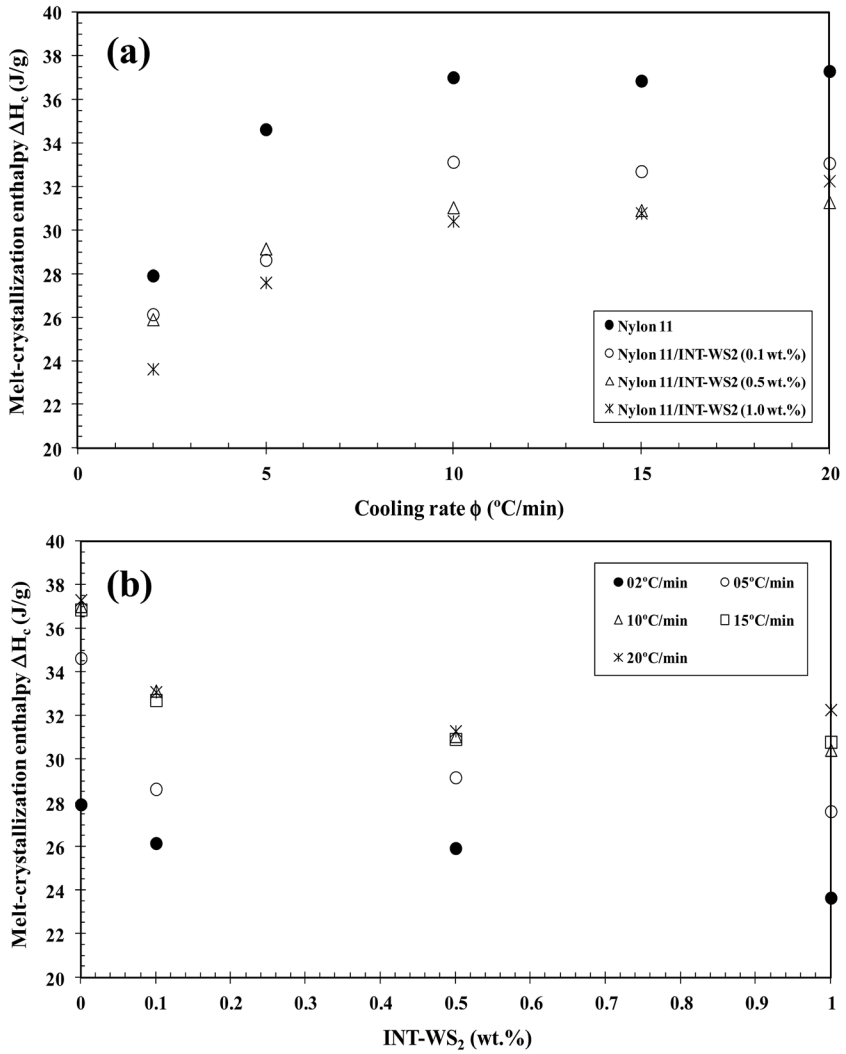

Fig. 5 Variation of the crystallization enthalpy (ΔH_c) of nylon 11/INT-WS_2 with (a) cooling rate and (b) composition.

nylon 11/INT-WS_2 nanocomposites improves with INT-WS_2 loading, indicating that the nanofiller is an efficient nucleating agent for nylon 11.

3.5. Effective energy barrier

To estimate the effective energy barrier for the transport of polymer chains towards the growing crystal surface, non-isothermal crystallization studies were carried out using DSC and the Kissinger model[41] applied to the data. Thus, the crystallization activation energy (ΔE) of the process could be calculated from the variation of peak temperature (T_p) with cooling rate (ϕ) as follows:

$$\ln\left(\frac{\phi}{T_p^2}\right) = \text{Constant} - \frac{\Delta E}{RT_p} \quad (3)$$

where R is the universal gas constant. The activation energies were calculated using the slopes of the lines obtained from plots of $\ln \phi/T_p^2$ against $1/T_p$ (Fig. 8). Values for ΔE of −334.1, −315.1, −300.8 and −302.0 kJ mol^{-1} were calculated for neat nylon 11 and nanocomposites with 0.1, 0.5 and 1.0 wt% INT-WS_2, respectively. The negative ΔE values demonstrate that the crystallization process is a barrierless and spontaneous, with the crystallization rate increasing with decreasing temperature. It is well-known that polymer chains are highly entangled in the melt and possess a relatively high viscosity and low diffusivity. Therefore, for polymer crystallization the polymer chains or segments must overcome certain energy barriers to transport (or diffuse) and deposit (or attach) onto the growing front of a crystal. As shown, the apparent ΔE values of the nanocomposites vary with the presence of INT-WS_2 in the range between −302 and −315 kJ mol^{-1}, indicating that the restriction of molecular mobility of n chains does not appear to be a limiting factor in the crystallization rate, demonstrating that the nucleation activity of INTs plays a dominant role in accelerating the crystallization of nylon 11.

3.6. Dynamic mechanical properties

Dynamic mechanical analysis (DMA) is sensitive to a wide range of polymer transitions and relaxation processes, and as such the effect of the nanocomposites on these processes. The storage

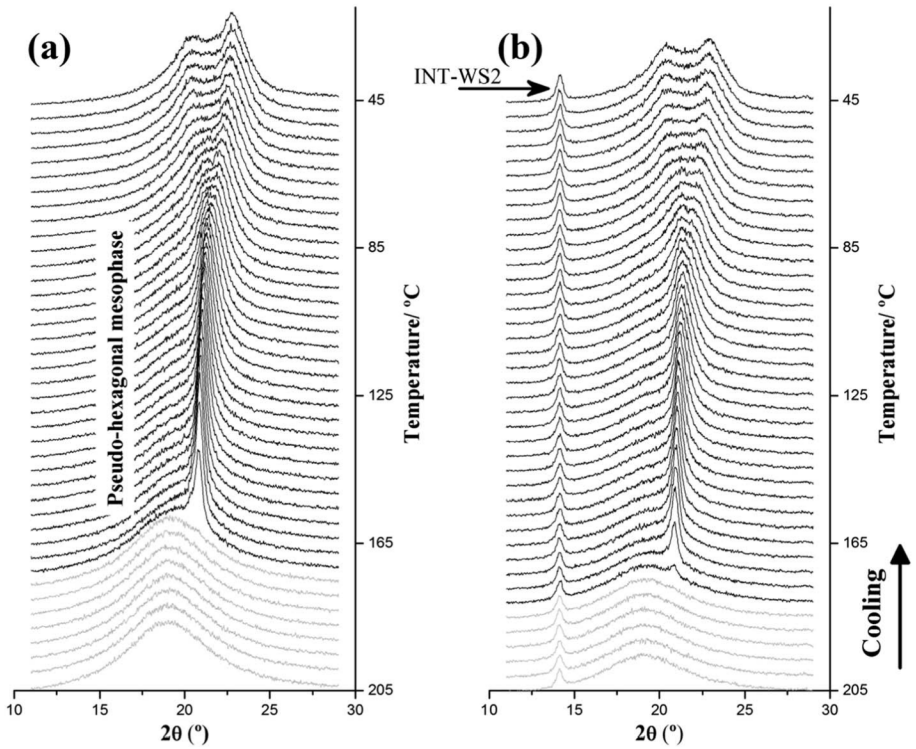

Fig. 6 WAXD diffractograms of the dynamic crystallization of (a) pure nylon 11 and (b) nylon 11/INT-WS_2 (1.0 wt%) obtained during cooling from the melt to room temperature.

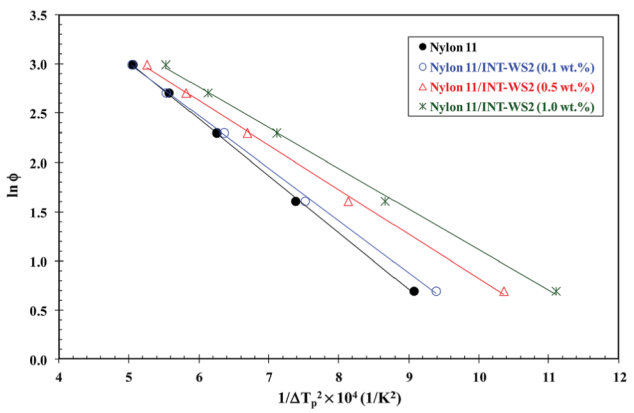

Fig. 7 Dobreva plots for nylon 11/INT-WS_2 nanocomposites.

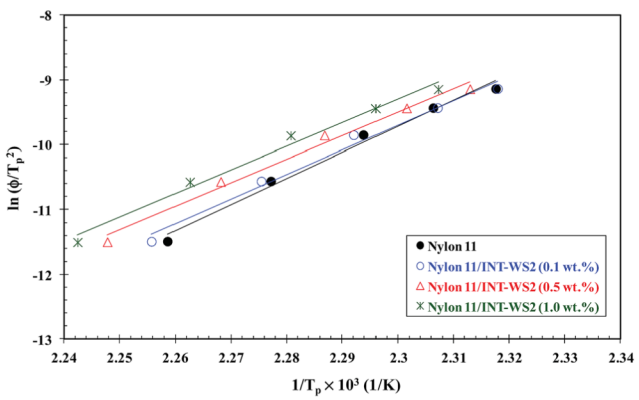

Fig. 8 Kissinger plots for nylon 11/INT-WS_2 nanocomposites.

modulus (E') and loss factor (tan δ) for neat nylon 11 and nylon 11/INT-WS_2 (1.0 wt%) nanocomposites at a frequency of 1 Hz are shown in Fig. 9a. It can be seen that the INT-WS_2 led to an increase in storage modulus of nylon 11 throughout all temperature range tested. The Fig. 9b shows the storage modulus values at room temperature (25 °C) as a function of INT-WS_2 concentration. As can be observed, the storage modulus of nylon 11 (1214 MPa) increases to 1236 MPa and 1273 MPa with 0.1 to 0.5 wt% INT-WS_2 respectively, thus indicating a slight improvement in stiffness due to the reinforcement effect of the well-dispersed rigid INTs. However, a further increase in the concentration of INT-WS_2 (*i.e.* 1.0 wt%) resulted in a negative impact on the mechanical performance of nylon 11. For nanofiller contents ≤0.5 wt%, the improvements in E' observed in this work are significantly lower than those reported for PLLA/INT-WS_2 and PEEK/INT-WS_2.[18,19] In these previous works, it was reported that the state of dispersion of the INT-WS_2 and its interfacial adhesion within the polymer matrix plays a vital role in property improvement of the dynamic mechanical properties of the resulting polymer/INT-WS_2 nanocomposites. In particular, in the case of the nanocomposite biomaterials based on PEEK and INT-WS_2, the storage modulus of polymer matrix was found to be greatly enhanced upon addition of increasing INT-WS_2 loadings due to the presence of strong INT-matrix interfacial adhesion.[19] Thus, it seems that only a slight enhancement of the storage modulus for nylon 11

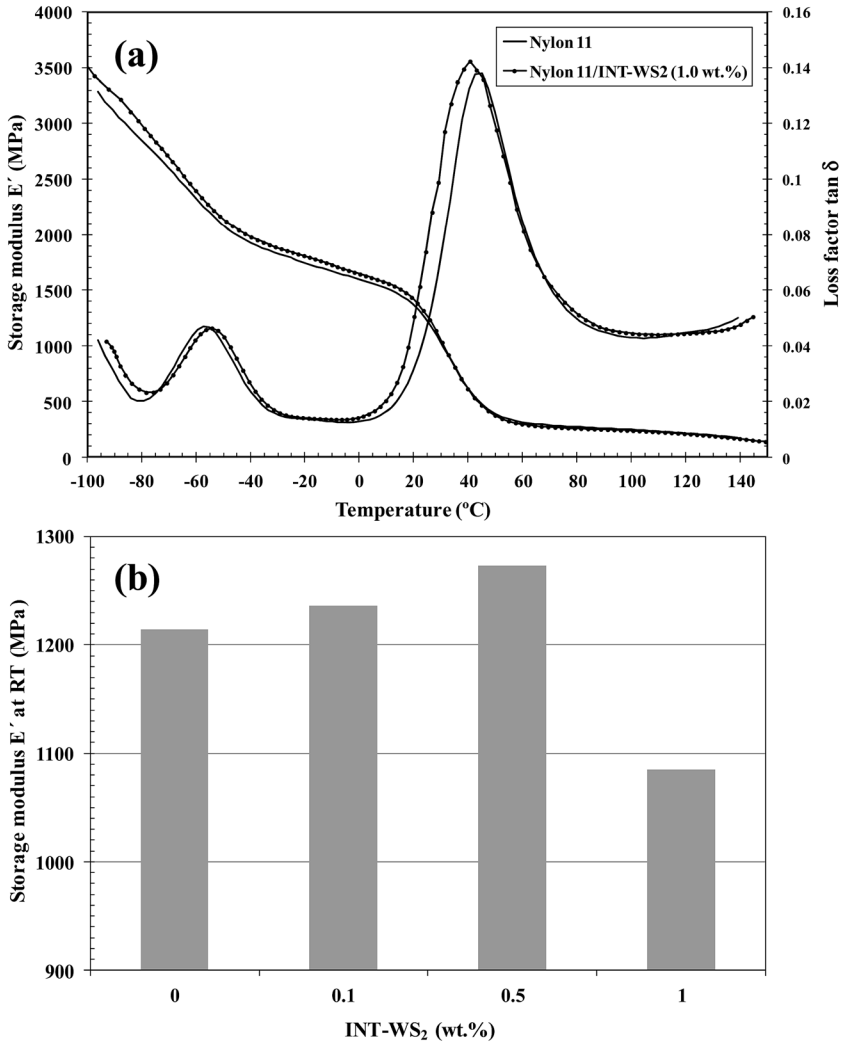

Fig. 9 (a) Dynamic mechanical spectra of nylon 11/INT-WS_2 nanocomposites obtained in the tensile mode at 1 Hz and (b) the room temperature values of storage modulus (E') of nylon 11 *versus* INT-WS_2 concentration.

with the nanotubes was observed due to the absence of, or poor interfacial interaction between the two components.

With regards to the loss factor (tan δ) results for different compositions, we observed that the incorporation of INT-WS_2 does not appear to have a significant effect on the temperature of the two relaxation processes of nylon 11 matrix in the temperature range −100 to 150 °C, namely the α and β transitions occurring at around 46 and −56 °C, respectively. However, the width of the tan δ peak increases significantly by almost 20%, from a full-width at half maximum (FWHM) value of 30.3 °C for nylon 11 to 36.0 °C with the incorporation of 1.0 wt% INT-WS_2. Furthermore, this broadening occurs over the lower temperature regions of the peaks, suggesting that the INT-WS_2 increases the heterogeneity of the amorphous phase towards regions of higher molecular mobility. This can be explained *via* the increased rate of crystallization for nylon 11/INT-WS_2 nanocomposites, which results in greater amorphous phase inhomogeneity compared to neat nylon 11. This observation is similar to that reported for nylon 11-barium titanate ($BaTiO_3$) nanocomposites (≤12 wt%), where it was concluded that the decrease of the cooperatively rearranging region (CRR) size could not be attributed to the polymer crystallinity, but rather that the increase of $BaTiO_3$ content results in an increase of hydrogen bond density that is coherent with the existence of the cooperative rearrangement of regions of smaller size.[41]

4. Conclusions

In the present investigation, analysis of the influence of INT-WS_2 on the dynamic crystallization kinetics of nylon 11 shows a significant dependence on INT-WS_2 content and cooling rate, whilst its crystalline structure remains unaltered. In particular, the crystallization temperature for the nylon 11/INT-WS_2 nanocomposites decreased with increasing cooling rate for a given INT-WS_2 content and increased with INT-WS_2 content for a given cooling rate. However, the addition of INT-WS_2 induces a decrease in the crystallization enthalpy of nylon 11. In the same way, the data of the nucleation activity and effective energy barrier reiterate that the INT nanofiller is an efficient nucleating agent for nylon 11. In particular, the disadvantage of the INT-WS_2 with respect to the

difficulty of the transport of nylon 11 macromolecular segments to the growing surface was outweighed by the nucleation attained in the presence of INT-WS_2. Both nylon 11 and nylon 11/INT-WS_2 nanocomposites undergo a polymorphic crystalline transition during cooling. The increase of the crystallization rate of nylon 11 in the nylon 11/INT-WS_2 nanocomposites induced the appearance of more-disordered phase at higher temperatures than in the case of neat nylon 11. On the other hand, the mechanical relaxation spectra of the nanocomposites were found to be very similar to those of neat nylon 11. In particular, analysis of the storage modulus of nylon 11 with INT-WS_2 concentration reveals a slight increase in the rigidity of the nylon 11 matrix. Additionally, broadening of the tan δ peak of nylon 11/INT-WS_2 occurs at a lower temperature with the incorporation of INT-WS_2. This fact is coherent with the increase of the heterogeneity of the amorphous phase towards regions of higher molecular mobility. The results obtained from the thermal and dynamic mechanical experiments, along with the good materials processability, economic and sustainability benefits, encourage further investigations in order to evaluate the full potential of these new nanocomposites for their potential use in eco-friendly and medical applications.

Acknowledgements

This work was supported by the Spanish Ministry Economy and Competitivity (MINECO), Projects MAT-2010-21070-C02-01 and MAT2013-41021-P. MN and PS would also like to acknowledge the MINECO for a 'Ramón y Cajal' Senior Research Fellowship and a Juan de la Cierva Postdoctoral Fellowship, respectively.

References

1 R. Tenne, L. Margulis, M. Genut and G. Hodes, *Nature*, 1992, **360**, 444–445.
2 L. Margulis, G. Salitra, R. Tenne and M. Talianker, *Nature*, 1993, **365**, 113–114.
3 C. N. R. Rao and M. Nath, *Dalton Trans.*, 2003, 1–24.
4 M. Remskar, *Adv. Mater.*, 2004, **16**, 1497–1504.
5 R. Tenne, *Nat. Nanotechnol.*, 2006, **1**, 103–111.
6 R. Tenne and M. Redlich, *Chem. Soc. Rev.*, 2010, **39**, 1423–1434.
7 A. Zak, L. Sallacan-Ecker, A. Margolin, M. Genut and R. Tenne, *Nano*, 2009, **4**, 91–98.
8 A. Zak, L. Sallacan Ecker, N. Fleischer and R. Tenne, *Sens. Transducers J.*, 2011, **12**, 1–10.
9 M. Naffakh, A. M. Díez-Pascual, C. Marco, G. Ellis and M. A. Gómez-Fatou, *Prog. Polym. Sci.*, 2013, **38**, 1163–1231.
10 R. Tenne, R. Rosentsveig and A. Zak, *Phys. Status Solidi A*, 2013, **210**, 2253–2258.
11 M. Pardo, T. Shuster-Meiseles, S. Levin-Zaidman, A. Rudich and Y. Rudich, *Environ. Sci. Technol.*, 2014, **48**, 3457–3466.
12 M. Naffakh, M. Remškar, C. Marco, M. A. Gómez and I. Jiménez, *J. Mater. Chem.*, 2011, **21**, 3574–3578.
13 E. Zohar, S. Baruch, M. Shneider, H. Dodiu, S. Kenig, D. H. Wagner, A. Zak, A. Moshkovith, L. Rapoport and R. Tenne, *Sens. Transducers J.*, 2011, **12**, 53–65.
14 C. S. Reddy, A. Zak and E. Zussman, *J. Mater. Chem.*, 2011, **21**, 16086–16093.
15 G. Lalwani, A. M. Henslee, B. Farshid, P. Parmar, L. Lin, Y. X. Qin, F. K. Kasper, A. G. Mikos and B. Sitharaman, *Acta Biomater.*, 2013, **9**, 8365–8373.
16 S. Kumar, C. Borriello, G. Nenna, R. Rosentsveig and T. Di Luccio, *Eur. Phys. J. B*, 2012, **85**, 160/1–7.
17 M. Naffakh, C. Marco and G. Ellis, *CrystEngComm*, 2014, **16**, 1126–1135.
18 M. Naffakh, C. Marco and G. Ellis, *CrystEngComm*, 2014, **16**, 5062–5072.
19 N. Naffakh and A. M. Díez-Pascual, *J. Mater. Chem. B*, 2014, **2**, 4509–4520.
20 N. D. Spiccia, E. Border, J. Illesinghe, W. R. Jackson and A. J. Robinson, *Synthesis*, 2013, 1683–1688.
21 M. Dhanalakshmi and J. P. Jog, *eXPRESS Polym. Lett.*, 2008, **2**, 540–545.
22 T. D. Fornes and D. R. Paul, *Macromolecules*, 2004, **37**, 7698–7709.
23 S. Huang, M. Wang, T. Liu, W. D. Zhang, W. C. Tjiu, C. He and X. Lu, *Polym. Eng. Sci.*, 2009, **49**, 1063–1068.
24 Y. Hu, L. Shen, H. Yang, M. Wang, T. Liu, T. Liang and J. Zhang, *Polym. Test.*, 2006, **25**, 492–497.
25 D. M. Panaitescu, A. N. Frone and C. Nicole, *Eur. Polym. J.*, 2013, **49**, 3857–3866.
26 D. Yuan, B. Wang, L. Wang, Y. Wang and Z.- Zhou, *Composites, Part B*, 2013, **55**, 215–220.
27 G. Hu, Y. Ma and B. Wang, *Mater. Sci. Eng., A*, 2009, **504**, 8–12.
28 M. L. Di Lorenzo and C. Silvestre, *Prog. Polym. Sci.*, 1999, **24**, 917–950.
29 Q. X. Zhang, Z. S. Mo, H. F. Zhang, S. Y. Liu and S. Z. D. Cheng, *Polymer*, 2001, **42**, 5543–5547.
30 I. S. Gunes, F. N. Cao and S. C. Jana, *Polymer*, 2008, **49**, 2223–2234.
31 I. S. Gunes, G. A. Jimenez and S. C. Jana, *Carbon*, 2009, **47**, 981–997.
32 M. Wu, G. Yang, M. Wang, W. Wang, W. D. Zhang, J. Feng and T. Liu, *Mater. Chem. Phys.*, 2008, **109**, 547–555.
33 Q. Zhang, M. Yu and Q. Fu, *Polym. Int.*, 2004, **53**, 1941–1949.
34 Z. Yang, S. Huang and T. Liu, *J. Appl. Polym. Sci.*, 2011, **122**, 551–560.
35 S. M. Aharoni, *n-Nylons, Their Synthesis, Structure, and Properties*, J. Wiley & Sons, Chichester, 1997.
36 S. S. Nair, C. Ramesh and K. Tashiro, *Macromolecules*, 2006, **39**, 2841–2848.
37 A. Mollova, R. Androsch, D. Mileva, C. Schick and A. Benhamida, *Macromolecules*, 2013, **46**, 828–835.
38 A. Dobreva and I. Gutzow, *J. Non-Cryst. Solids*, 1993, **162**, 1–12.
39 A. Dobreva and I. Gutzow, *J. Non-Cryst. Solids*, 1993, **162**, 13–25.
40 S. Y. Liu, Y. N. Yu, Y. Cui, H. F. Zhang and Z. S. Mo, *J. Appl. Polym. Sci.*, 1998, **70**, 2371–2380.
41 J. F. Capsal, C. Pousserot, E. Dantras, J. Dandurand and C. Lacabanne, *Polymer*, 2010, **51**, 5207–5211.